EARTH SCIENCES
RESEARCH JOURNAL
Earth Sci. Res. J. Vol. 27, No. 4 (December, 2023): 367 - 379

UNIVERSIDAD NACIONAL DE COLOMBIA

GEOLOGY

Mapping hydrothermal alterations and associated lineaments within Kaiama, north-central Nigeria, using Landsat 8 Operational Land Imager Data and Digital Elevation Model

Umaru Aliyu Ohiani[1,2]* Olugbenga Okunlola[3], Umaru Adamu Danbatta[4] and Olusegun G. Olisa[5]
1. Pan African University of Life and Earth Science Institute, including (Health and Agriculture), University of Ibadan, Nigeria
2. Department of Geology, University of Maiduguri, Maiduguri, Borno State, Nigeria
3. Department of Geology, Faculty of Science, University of Ibadan, Nigeria
4. Department of Geology, Faculty of Physical Sciences, Ahmadu Bello University, Nigeria
5. Department of Earth Sciences, Olabisi Onabanjo University, Ago Iwoye, Ogun State, Nigeria
*Corresponding author: umaru.aliyu@paulesi.org.ng

ABSTRACT

This research focuses on the geological investigation of Kaiama region, which is characterized by a diverse range of rock formations, including mylonites, porphyritic granites, gneiss, schist, phyllites, and pink granites. The study employs remote sensing techniques, utilizing Landsat 8 OLI data and Digital Elevation Models, to systematically map the spatial distribution of hydrothermal alterations and tectonic structures associated with mineralization in the Kaiama area. Various image processing methods such as Color Composites, Band Rationing, and Principal Component Analysis (PCA) were employed to extract valuable information from the collected datasets. Utilizing Sabins band ratios (4/2, 6/7, and 6/5), we categorized alterations associated with iron oxides, clay minerals, and ferrous minerals. PCA was applied to refine the identification of alteration zones, using two distinct sets of images: H-image (comprising bands 2, 4, 5, and 7) and F-image (comprising bands 2, 5, 6, and 7), which represented iron-oxide and hydroxyl mineral deposits, respectively. The synthesis of H, F, and H+F images in RGB format provided an optimal representation of the spatial distribution of hydrothermal alterations, exhibiting a strong positive correlation with known mining regions for gold, copper, wolframite, and tantalite within the study area. Furthermore, a comprehensive analysis of regional lineaments revealed a consistent NNE-SSW to NE-SW correlation, suggesting a predominant control on mineralization trends. This study advocates for adopting remote sensing techniques, specifically Landsat 8 data and DEM, as an effective approach for mapping hydrothermal alterations and identifying key structural controls associated with mineralization.

Keywords: Band Ratio, Principal Component Analysis, False Colour Composite, Landsat 8 OLI, Kaiama

Levantamiento de mapas de alteraciones hidrotermales y lineamientos asociados al interior de Kaiama, norte central de Nigeria, con información del satélite Landsat 8 Operational Land Imager y Modelos Digitales de Elevación

RESUMEN

Este trabajo se enfoca en la investigación geológica de la región de Kaiama, la cual se caracteriza por un rango diverso de formaciones rocosas que incluyen milonitas, granitos porfiríticos, gneises, esquistos, filitas y granitos rosa. El trabajo emplea técnicas de teledetección, con información del satélite Landsat 8 OLI y Modelos Digitales de Elevación, para levantar un mapa de la distribución espacial de las alteraciones hidrotermales y las estructuras tectónicas asociadas con la mineralización del área de Kaiama. Se emplearon varios métodos de procesamiento de imágenes como Falso Color Compuesto, Reducción de Bandas, y Análisis de Componentes Principales para determinar la información importante del conjunto de datos recolectados. Los autores utilizaron los ratios de la banda de Sabins (4/2, 6/7, y 6/5) para categorizar las alteraciones asociadas con los óxidos de hierro, los minerales arcillosos y los minerales ferrosos. El Análisis de Componentes Principales se aplicó para refinar la identificación de las zonas de alteración a través de dos configuraciones de imágenes: Imagen H (que comprende las bandas 2, 4, 5 y 7) e Imagen F (que comprende las bandas 2, 5, 6 y 7), los cuales representan los depósitos de óxidos de hierro y de minerales hidróxidos. La combinación de las imágenes H, F, y H+F en el formato RGB proveyó una representación óptima de la distribución espacial de las alteraciones hidrotermales y mostró una fuerte correlación positiva con regiones mineras caracterizadas de oro, cobre, wolframita y tantalita en el área de estudio. Además, un análisis extenso de los lineamientos regionales revelaron una correlación consistente NNE-SSO hacia NE-SO, lo que sugiere un control predominante en las tendencias de mineralización. Este estudio propone la adopción de técnicas de teledetección, especificamente el uso de información del satélite Landsat 8 y Modelos Digitales de Elevación, como un acercamiento efectivo para levantar mapas de alteraciones hidrotermales e identificar las claves de control estructurales asociadas con la mineralización.

Palabras clave: Reducción de Bandas; Análisis de Componentes Principales; Falso Color Compuesto; Landsat 8 OLI; Kaiama.

Record
Manuscript received: 29/01/2023
Accepted for publication: 04/01/2024

How to cite this item:
Ohiani, U. A., Okunlola, O., Danbatta, U. A., & Olisa, O. G. (2023). Mapping hydrothermal alterations and associated lineaments within Kaiama, north-central Nigeria, using Landsat 8 Operational Land Imager Data and Digital Elevation Model. Earth Sciences Research Journal, 27(4), 367-379. https://doi.org/10.15446/esrj.v27n4.107002

1. Introduction

Numerous scientific investigations have demonstrated the intrinsic value and efficacy of remote sensing techniques in the realm of geological and mineral exploration endeavors, with a particular emphasis on various metallic and non-metallic mineral deposits (Ahmadi and Uygucgil, 2021). When conducting in-depth exploration and exploitation of specific mineral deposits, it becomes imperative to meticulously consider the spatial distribution of hydrothermal alterations associated with those deposits (Amara et al., 2019). Consequently, remote sensing play a crucial role in the choice of the mineralized sites. This approach has become acknowledged as best practice when leading most geological expeditions due to its high effectiveness, low cost, and time-saving qualities (Yekin, 2003).

In remote sensing, multispectral and hyperspectral satellite and aerial sensors are used to monitor the reflection and absorption of matter on the Earth's surface (Maleki *et al*., 2021). Minerals are then targeted using a variety of enhancement techniques based on their spectral signature (Wang *et al*. 2020; Guha *et al*. 2020). The use of remote sensing imagery has been adopted globally and widely employed in mapping the spatial distribution of hydrothermal alterations within diverse metallogenic provinces (Pour and Hashim, 2011; Pour *et al*., 2013; Amara *et al*., 2019; Osinowo *et al*., 2021; Frutuoso *et al*., 2021; Maleki *et al*., 2021; Ahmadi and Uygucgil, 2021; Andongma *et al*.,2021; Ombiro *et al*.,2021; Umaru *et al.,* 2022; Abdulmalik *et al*., 2021; Aliyu *et al.,* 2021). Landsat data, in particular, have gained extensive traction in the realms of structural and geological mapping, as well as hydrothermal alteration mapping, owing to the presence of mid-infrared bands that exhibit discernible spectral characteristics aligning with a majority of hydrothermal minerals (Ducart *et al*., 2016; Umaru *et al*., 2021).

Through its Operational Land Imager (OLI) sensor, which covers a wavelength range of 0.4-2.3 m, it is possible to identify mineral assemblages of hydroxyl and iron-oxide bearing (Ducart *et al*., 2016). In many instances, a remote sensing analysis of a specific region becomes imperative to delineate hydrothermal zones and refine target locations prior to embarking on field-based, geochemical, or mineralogical investigations. The area under investigation (Kaiama) has developed into an intriguing mining site due to the existence of several mineral deposits including wolframite, tantalite, cassiterite, copper, and gold whose extent of occurrence and spatial distribution is not fully documented (Dada and Ajadi, 2018; Alepa *et al*., 2019a, 2019b).

Within the study region, there has been a limited exploration of remotely sensed data for the identification of hydrothermal alteration zones, which could serve as a valuable tool for regional exploration to unlock the full mineralization potential of the area. Previous remote sensing studies conducted in the region have primarily focused on a regional scale, involving the spatial mapping of hydrothermal alterations and structural features, with a particular emphasis on gold and cassiterite mineralization (Ige *et al.,* 2022). Additionally, there have been reconnaissance geochemical investigations aimed at assessing the distribution of ore-forming components and the potential for mineralization in the Kaiama area (Alepa *et al.,* 2019a; 2019b).

The primary objective of this study is to utilize remote sensing methods, specifically leveraging Landsat 8 OLI data and a digital elevation model, on an expansive scale to systematically delineate hydrothermal alteration zones and tectonic lineaments within the study area. This aims to provide a foundation for further exploration techniques that can be employed to fully realize and develop the mineralization potential of the region. To achieve these objectives, the authors have implemented three well-established and reliable image processing techniques: color composites, band ratios, and Principal Component Analysis (PCA). These methods are employed for the precise mapping of target features, including alteration zones. Additionally, an automated approach is used to extract tectonic lineaments from Digital Elevation Model data. Generally, we enhance alteration zones, second- and third-order faults, and analyze their association with mineralization using satellite images while detailed field mapping was done to validate the remote sensing results.

2. Geographical and geological setting

Kaiama is a local government in Kwara State of Nigeria and it is bounded to the north by Niger state, to the south by Oyo State and share a boundary to the west with Benin Republic (Figure 1A and 1B). The area is underlain by mylonites, porphyritic granites, granite gneiss, talc schist, phyllites and pink granites (Figure 1C). These rocks form part of the southwestern basement complex of Nigeria which constitutes the migmatite gneiss complex, the schist belts and the older granitic rocks as well as undeformed acid and basic dykes. The migmatite-gneiss complex is generally considered as the basement complex "Senso Stricto" as the oldest basement (Rahman, 1988; Dada, 2006). About half of the Nigerian basement consists of the migmatite-gneiss complex. It is a heterogeneous assemblage including migmatised gneisses, banded gneisses, granitic gneiss and a series of metamorphosed basic and ultrabasic rocks. These rocks strongly resemble the Tonalite-Trondhjemite-Granodiorite (TTG) suites of Archean and Early Proterozoic terrains elsewhere in the world (Dada *et al*., 1993). The gneisses of the migmatite-gneiss complex are interleaved with amphibolites that may be derived from Mg-rich rocks such as continental basalts (Caby *et al*., 1990; Dada,1999; Dada, 2008). Oyawoye (1972) noted that the banded gneisses are possibly the oldest rocks in the country, older than granite gneiss that yielded a Rb-Sr whole-rock isochron age of 2190 ± 30 Ma. Ajibade (1980) distinguished the ancient migmatites in northern Nigeria from the Pan-African migmatites by their complex polyphase deformation and mylonitization.

The schist belts comprise suits of the metasedimentary and metavolcanic rocks. McCurry, (1976) distinguished the rocks of the schist belts into "Older Metasediments" and "Younger Metasediments". The Older Metasediments are high-grade remnants in the gneisses and migmatites and are believed to have been formed about 2,500 Ma (McCurry, 1976). They consist of calc-silicate rocks, arkosic quartzite and high-grade schist that occur as lensoid relics in the regional gneisses or as paleosomes of migmatites (Danbatta, 2008). The Younger Metasediments are low-grade sediment-dominated schist groups and are composed mainly of pelitic and semi-pelitic schist, meta conglomerate, quartzite, calc-silicate rock, marble, mafic to ultramafic rocks, acid to intermediate volcanic rocks and rare banded iron formations (Danbatta, 2008). In the western half of the country, they occur as discontinuous north-south trending belts within the basement. The older granites comprise the syntectonic to late tectonic granitoid that intrude into both the migmatite-gneiss complex and the metasediments. They include rocks varying in composition from granite to tonalite and charnockites with smaller bodies of syenite, gabbro and pegmatite (Woakes *et al.,* 1987). The granitoids have yielded radiometric ages in the range of 750-500 Ma which lies within the Pan-African spectrum. These Pan-African granitoid are referred to as the Older Granites in Nigeria to distinguish them from the Mesozoic anorogenic granite ring- complexes (the Younger Granites).

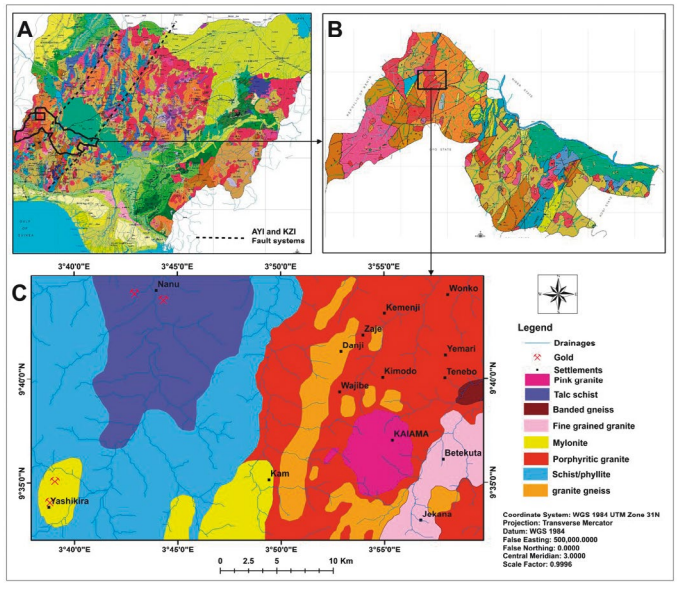

Figure 1. A. Geological map of Nigeria showing the location of Kwara State, B). Geological map of Kwara State showing the location of Kaiama, C). Geological map of Kaiama

3. Materials and methods

Remote sensing data acquisition

In this investigation, a cloud-free level 1T Landsat 8 OLI/TIRS (Path 191/Row 53) sensor imagery covering the analyzed area and acquired on 10 February 2022 was used. It was downloaded from the USGS EROS website, http://earthexplorer.usgs.gov, with eleven (11) bands and orthorectified. The spectral bands include a panchromatic band with a resolution of 15 meters, a visible band with a resolution of 30 meters, three infrared bands (NIR, SWIR1, and SWIR2 at 30 meters), a cirrus band with a resolution of 30 meters, an aerosol band with a resolution of 30 meters, and two thermal infrared bands at 30 meters. The performance characteristics of Landsat 8 OLI is shown in (Table 1). Hydrothermal alteration mapping was conducted utilizing Landsat 8 Operational Land Imager (OLI) data. The Digital Elevation Model (DEM) utilized in this research was sourced from the ALOS-PALSAR sensor, established in 2006 by the Ministry of Economy, Trade and Industry (METI) and the Japan Aerospace Exploration Agency (JAXA). ALOS-PALSAR serves multiple purposes, including aiding geological studies and environmental conservation (Bannari *et al.* 2016). Acquired from the Alaska Satellite Facility (https://asf.alaska.edu/), the ALOS-PALSAR DEM boasts a resolution of 12.5 meters. Recent studies (Das *et al.* 2018; Gaikwad *et al.* 2023) have underscored its efficacy, reliability, and accuracy in delineating lineaments. Processing the DEM involved the use of ArcMap v.10.8 software, enabling the creation of four shaded relief images that accentuate the topographic and geomorphological features of the research area. The short wave infra-red region of Landsat 8 has a unique application to geological studies. For example, band 7 coincides with the absorption band caused by hydrous minerals such as clays mica, some oxides, and sulfates which makes them appear darker. Band 6 is used for soil and rock discrimination such as ferric iron or hematite rocks, and band 4 is used for the discrimination of soil from vegetation and delineation of soil cover (Nait Amara *et al.*,2019). Maps were created using ArcMap 10.8 while satellite data was processed using the ENVI 5.3 and the LINE module in PCI Geomatica 2018.

Preprocessing Landsat 8OLI data

Environment for Visualizing Images (ENVI) software version 5.3 was used to preprocess Landsat 8OLI data. Preprocessing was carried out in stages. A radiometric adjustment to calibrate the image data to radiance, reflectance, and brightness temperature as well as reducing image digital number errors. Atmospheric correction, to correct the impacts of the atmosphere as detected by the sensor. Minimum Noise Fraction (MNF) to detect the underlying dimension of picture data, segregate and normalize the noise present, raise the signal-to-noise ratio, and decrease computational demands for subsequent processing (Jensen, 2005; Nait Amara *et al*., 2019). To achieve the above preprocessing steps, Landsat calibration and Fast Line of Sight Atmospheric Analysis of Spectral Hypercubes algorithms (FLAASH) tools of ENVI software was applied. Finally, the Area of Interest (AOI) was then sub-setted from the Landsat scene.

Table 1. Spectral characteristics of Landsat-8 (Operational Land Imager (OLI) and Thermal Infrared Sensor (TIRS)) scene used in the current study

BANDS	BANDWIDTH (µm)	WAVELENGTH C ENTER (µm)	SPATIAL RESOLUTION (m)
Coastal/ aerosol)	0.435-0.451	0.4430	30
Blue	0.452-0.512	0.4820	30
Green	0.533-0.590	0.5615	30
Red	0.636-0.673	0.6545	30
NIR	0.851-0.879	0.860	30
SWIR-1	1.566-1.651	1.6085	30
SWIR-2	2.107-2.294	2.2005	30
Panchromatic	0.503-0.676	0.5895	15
Cirrus	1.363-1.384	1.3735	30
TIRS-1	10.60-11.19	10.8950	100
TIRS-2	11.50-12.51	12.005	100

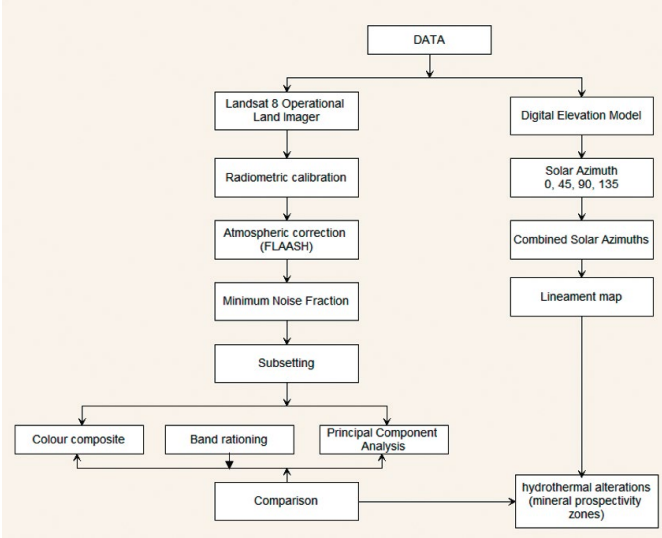

Figure 2. Flow chart for preprocessing and processing of Landsat 8 OLI and Digital Elevation Model data

Processing Landsat 8 OLI image

The Landsat 8OLI satellite data was processed to create images that emphasize geological features while minimizing background interference. Spectral and spatial patterns associated with hydrothermal alterations were delineated using processing techniques such as Color Composite (CC), Band Ratios (BR) and Principal Component Analysis (PCA). Furthermore, Digital Elevation Model (DEM) was employed to generate lineaments through an automated method. The entire processing workflow is illustrated in Figure 2.

Color Composite (CC)

Color compositing involves the merging of grayscale Landsat data into an RGB channel, resulting in a multispectral image with multicolor representations. This combination can be a true color composite (TCC) or a false color composite (FCC). A TCC is created by combining the visible bands of the electromagnetic spectrum, while an FCC is produced when non-visible bands are composited. The resulting composite image has the ability to reveal details such as lithological boundaries, hydrothermal changes, vegetation, and soil characteristics, among others (Nait Amara et al., 2019). Numerous researches have employed color composites to identify hydrothermal alterations, utilizing combinations like RGB 567 (Yerkin, 2003), RGB 752 (Pour and Hashim, 2011), RGB 573 (Mia and Fujimitsu, 2012), and RGB 657 (Ali and Pour, 2014). In our study, we utilized a color composite of bands 5, 6, and 7 in the RGB spectrum to effectively highlight hydrothermal alterations within the study area.

Band Rationing (BR)

Band ratio technique is used to improve contrast and enhance compositional information while suppressing unwanted information. The technique involves dividing digital numbers, or the brightness values corresponding to the peaks of high and low reflectance curves of one band, by that of another band hence, highlighting geological features that are not visible in raw data (Pour and Hashim, 2015). Several writers have used band ratios approaches for geological usage to highlight minerals linked with hydrothermally altered rock based on the spectral reflectance and absorption of features (Table 2). For the purpose of this work, the Sabins ratio involving Band 4/2 will be used for mapping out iron oxides alterations (Sabins, 1999; Ali and Pour, 2014; Sekandari *et al*., 2020), band 6/7 for mapping alunite and clay minerals (Sabins, 1999; Ali and Pour, 2014; Pour and Hashim, 2015) and band 6/5 will be used for mapping ferrous minerals (Mia and Fujimitsu, 2012); Ali and Pour, 2014).

Table 2. Tested band ratios for Landsat 8 Operational Land Imager (OLI)

Band ratio	Feature
4/2	Iron oxides
6/7	Alumina and clay minerals
6/5	Ferrous minerals

Principal Component Analysis (PCA)

PCA is a technique for mapping lithological and alteration characteristics. It is a multivariate statistical technique that selects uncorrelated linear combinations of variables (eigenvector loadings), allowing each component to extract a linear combination with a smaller variance one at a time (Farahbakhsh *et al*., 2016; Takodjou Wambo *et al*., 2020). According to Crosta and Moore (1989) and Loughlin (1991), a PC image with moderate to high eigenvector loading for diagnostic reflectance and absorptive bands of a mineral or mineral group with opposite signs enhances that mineral. If the loading is positive in the mineral's reflective band, the picture tone for the enhanced target mineral will be bright; if it is negative, it will be dark. Therefore, eigenvector loading in each PCA would provide the PC image that contains the spectral data of the mineral under study. Although this information typically only makes up a very small portion of the original bands' total information content, it is anticipated that the loaded information will reveal the desired mineral's spectral signature (Jensen, 2005; Gupta, 2017).

Lineament extraction

Digital Elevation Models (DEM) have been used in several research for the extraction of geological lineaments (Koike *et al*., 1998; Masoud and Koike, 2017; Meixner *et al*., 2018; Umaru *et al*., 2021; Andongma *et al*., 2021). The use of digital elevation models has the advantage of representing the true reap projections with no distortion, also a relief is clearly represented by tonal variations, and the position of the sun can be varied in most case. The DEM provides a better resolution when compared with other satellite imageries like LANDSAT and ASTER (Anwar *et al*., 2010; Mavoungou *et al.,* 2023). This study employed the use of DEM to extract lineaments associated with the investigated area. Four shaded relief images were generated representing four different solar azimuths (0, 45, 90 and 135 degrees respectively). An ambient light setting of 0.20 was selected to produce a good contrast. The ambient light setting is a scaling factor in Erdas Imagine program (Erdas, 1998). The shaded relief images created were combined to produce one shaded relief image using GIS overlay algorithm in ArcMap software. The combined image was then used for the automatic lineament extraction on PCI Geomatica software following the default setting in Table 3. A rose diagram generated from the lineaments was used to show the preferred structural orientation for mineralization.

Table 3. Default parameter for lineament extraction on PCI Geomatica

NAME	DESCRIPTION	VALUES
RADI	Radius of filter in pixels	12
GTHR	Threshold for edge gradient	90
LTHR	Threshold for curve length	30
FTHR	Threshold for line fitting error	10
ATHR	Threshold for angular difference	30
DTHR	Threshold for linking distance	20

Results and discussion

Colour Composite

Figure 3 is the colour composite image of the study area. It was produced by assigning bands 5 (0.851-0.879µm) in red channel, band 6 (1.566-1.651µm) in green channel and band 7 (2.107-2.294µm) in blue channels. The resultant image shows the general hydrothermal alterations of the study area in white, dark blue and light green pixels.

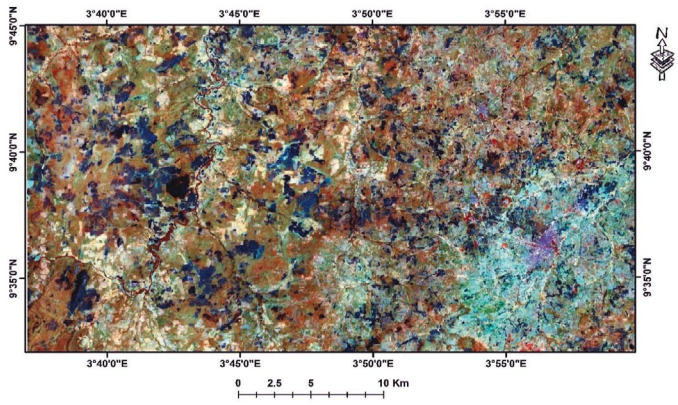

Figure 3. Color composite image RGB combination of bands 5, 6, and 7

Band Ratio

Figure 4 represents a band ratio of 4/2, emphasizing regions where iron oxide minerals are present pervasively or as surface coatings. In this image, iron oxide-rich areas are depicted as bright or white pixels, while regions with lower iron oxide content appear as dark or black pixels. This distinction arises from the optical properties of iron-bearing minerals: they exhibit high reflectance in band 4 and strong absorption in band 2. As evident in the ratio image, the prevalence of iron oxide-rich areas is most pronounced in the northern sections, extending southward toward the southwestern portion of the area. Figure 5 shows the ratio image of band 6/7 for clay and hydroxyl-bearing minerals. This emphasis arises from the pronounced reflectance in band 6 and significant absorption in band 7 exhibited by these minerals. Notably, the western part of the image is predominantly characterized by bright or white pixels, signifying the prevalence of these minerals. At the same time, darker areas correspond to regions with lower concentrations of clay or hydroxyl-bearing minerals.

The ratio 6/5 (Figure 6) mapped the regions of ferrous minerals represented as bright or white colors due to high reflectance of band 6 and high absorbance of band 5. This region occupies the southeastern parts underlain by fine grained granites. The combined band ratios image of 4/2, 6/7 and 6/5in RGB sequence known as Sabins ratio is represented in Figure 7. This image clearly revealed and delineate the spatial distribution of iron oxide rich areas, clay and hydrous minerals areas as well as ferrous minerals in blue, green and purple colors. Iron oxide minerals are most prevalent in the southwestern portion of the map progressing extending upwards into the northern area where they are associated with mylonites, talc schist and partly with phyllites. Clay and hydroxyl-bearing zones are distributed across the entire map in patchy patterns but conspicuously absent from the southeastern edge, which is primarily characterized by the presence of ferrous minerals found in association with fine-grained granites.

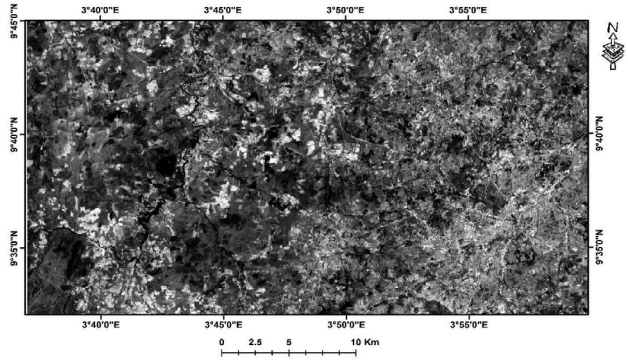

Figure 4. Band ratio 4/2 image highlighting regions of iron oxide in white or bright pixels

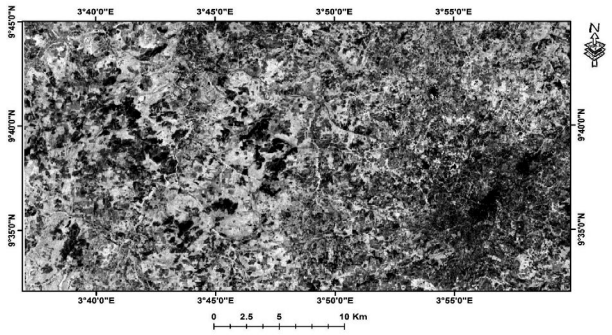

Figure 5. Band ratio 6/7 image highlighting regions of alunite and clay minerals in white or bright pixels

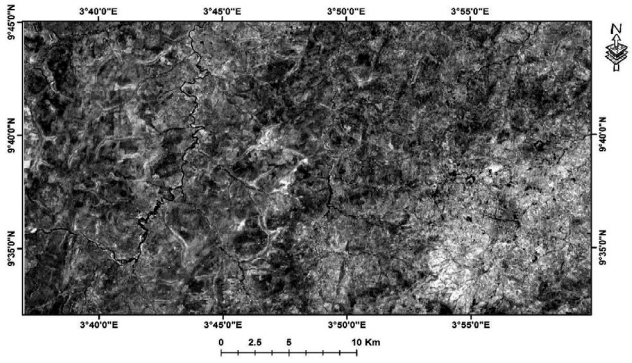

Figure 6. Band ratio 6/5 image highlighting regions of ferrous minerals in white or bright pixels

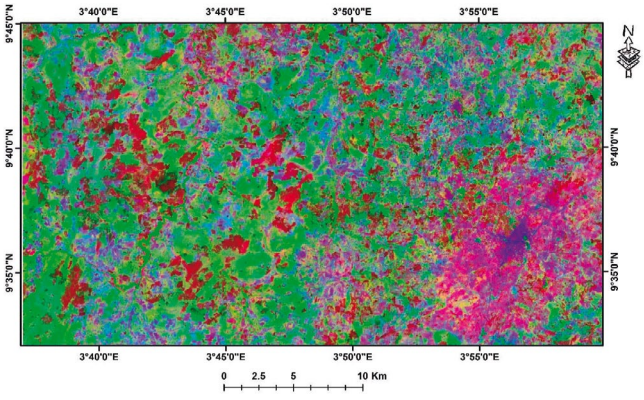

Figure 7. Band ratio composite image of 4/2, 6/7 and 6/5 (Sabins composite image) showing the spatial distribution of iron oxide, clay and hydrous minerals as well as ferrous minerals in purple, green and blue colours

Principal Component Analysis

In accordance with spectral analyses utilizing the spectral signatures of iron oxides and hydroxyl-bearing minerals derived from the USGS spectral library, a selection was made to utilize bands 2, 4, 5, and 6 of the Landsat 8 OLI sensors to accentuate the spectral characteristics associated with iron-oxide-bearing minerals. Simultaneously, bands 2, 5, 6, and 7 were employed to enhance the spectral signatures of hydroxyl-bearing minerals. Principal component analysis (PCA) was applied to transform the chosen bands into their respective principal components. Consequently, the outcomes of this transformation effectively delineated regions rich in OH-bearing minerals and iron minerals, respectively. Tables 4 and 5 represent the eigenvectors and eigenvalues from Crosta analysis of the Landsat 8 data. Examining the eigenvector values of the PCA loading for the selected bands 2, 4, 5, and 6 for iron oxides, shows that PC4 showed a clear contrast between bands 2 (0.77234) and 4 (-0.55141) (Table 4). Thus, PC4 highlighted the alteration areas in dark tone as a perfect contrast between eigenvectors of bands 4 and 2 due to the negative contribution from band 4 (Figure 8). The resultant PC4 image was then negated to produce a H-image based on Crosta and Moore classification (OH-bearing minerals) in bright or white colour for better identification (Figure 9).

Also, PCA was applied to selected bands 2,4,6 and 7 to map out regions of OH bearing minerals. Result showed that PC4 had the highest loading between the eigenvectors of band 6 (0.57130) and band 7 (-0.11447) (Table 5) hence revealing areas of high OH minerals in dark pixels due to the negative contribution from band 7 (Figure 10). Negating the image produced the Crosta and Moore (1989) F-image of the study area which is presented in bright colours for ease of identification (Figure 11). (Figure 12) is the combined image of H and F that shows the altered areas of iron oxides and hydroxyl minerals in bright tones called Crosta and Moore (1989) H+F image. After obtaining H, F and H+F images in a grey scale, a color composite image "Crosta alteration image" was generated after utilizing the OH-bearing minerals (H-image) in the red channel, the iron-bearing oxides (F- image) in the blue channel and the H+F image in green. The resulting hydrothermal alteration from this combination is presented in (Figure 13). The figure shows that iron oxide minerals are represented in dark blue colours, while hydroxyl bearing minerals are in brown to yellow colours. The regions of white pixels to light blue pixels notable as (combined iron and hydroxyl minerals) are delineated as the hydrothermal alteration zones and regarded as the zones of highest possibility for mineral occurrence (Figure 12).

Figure 14 provides a clear depiction of delineated hydrothermal alteration zones, with prominent hydrothermally altered areas concentrated in the southeastern region and appearing as distinct patches in the eastern part. The spatial distribution of the alteration zones strongly suggests their association with major structural features (lineaments), indicating a structural control on their distribution. The representation of these hydrothermal alteration zones on the geological map of the study area (Figure 19) further reveals their predominant occurrence within fine-grained granites, granite gneiss, pink granites, and mylonitic zones. This map also illustrates the close proximity of many hydrothermal alteration zones to pre-existing structural features, affirming the significant influence of structural factors on the spatial distribution of these hydrothermally altered minerals. Notably, when plotting the sites of mineralization such as copper, gold, tantalite, and wolframite onto the map, it becomes evident that these mineralization sites either closely coincide with the hydrothermal zones or directly overlap with them.

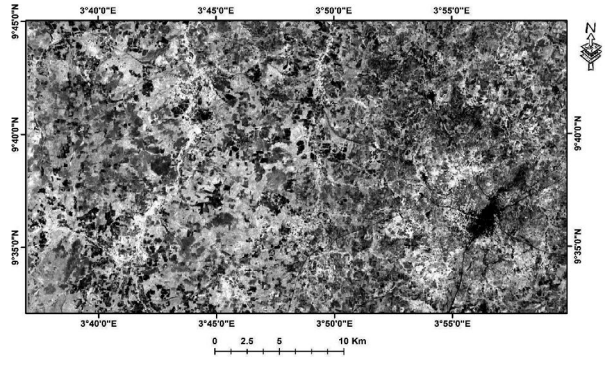

Figure 8. PC4 showing iron-oxide alteration areas in dark or black pixels

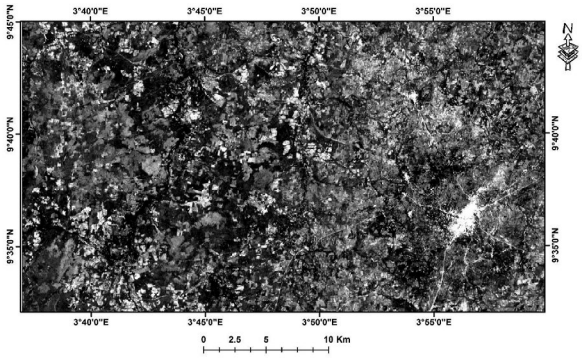

Figure 9. Negated Iron-oxide (H-image) showing alteration areas in bright or white pixels

Table 4. Eigenvalues and Eigenvectors loadings for iron oxide mapping Number of Input Layers=4, Number of Principal Component Layers=4

	BAND 2	BAND 4	BAND 5	BAND 6	% EIGENVALUES
PC1	0.09090	-0.06738	0.42980	0.89581	92.4386
PC2	0.31004	-0.06842	0.84015	-0.43971	5.6356
PC3	0.54691	0.82869	-0.10451	0.05698	1.8147
PC4	0.77234	-0.55141	-0.31384	0.03073	0.1111

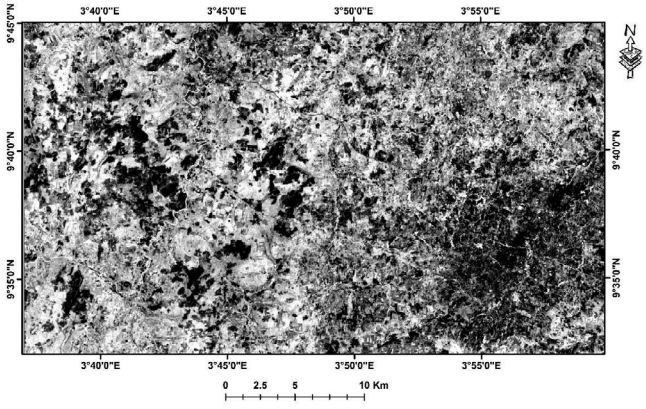

Figure10. PC2 showing hydroxyl alteration areas in black or dark pixels

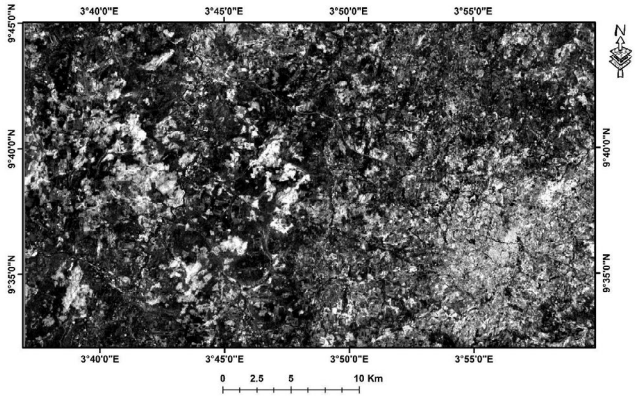

Figure 11. Negated hydroxyl minerals (F-image) represented in bright or light pixels

Table 5. Eigenvalues and Eigenvectors loadings for hydroxyl mapping Number of Input Layers=4, Number of Principal Component Layers=4

	BAND 2	BAND 5	BAND 6	BAND 7	% EIGENVALUES
PC1	0.08463	-0.03333	0.17039	0.98117	85.7715
PC2	0.44475	0.68022	0.57130	-0.11447	12.2666
PC3	0.68993	0.15200	-0.70446	0.06799	1.7388
PC4	0.56483	-0.71630	0.38511	-0.13993	0.2231

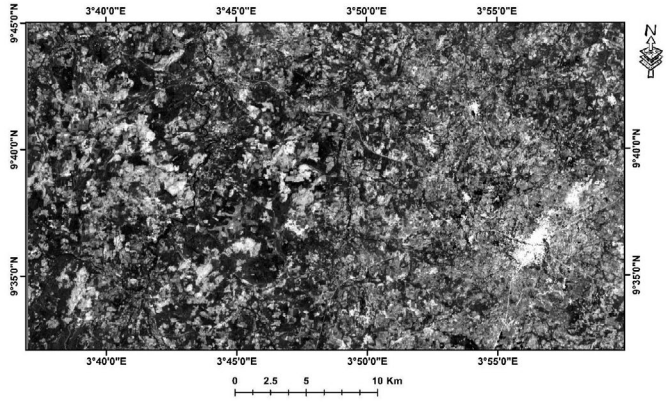

Figure 12. Combined hydroxyl and iron minerals as an H+F Image

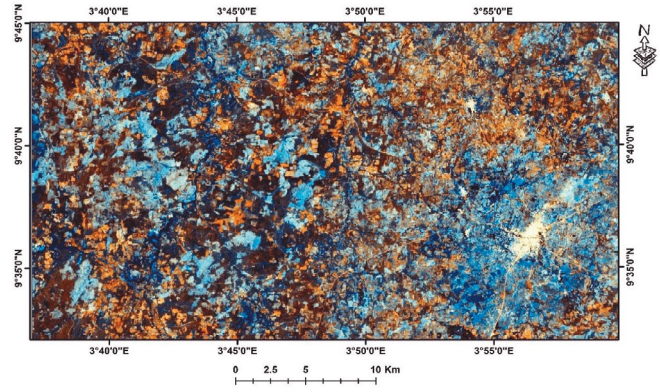

Figure 13. Crosta map (Alteration map) produced by compositing H, F and H+F images in RGB

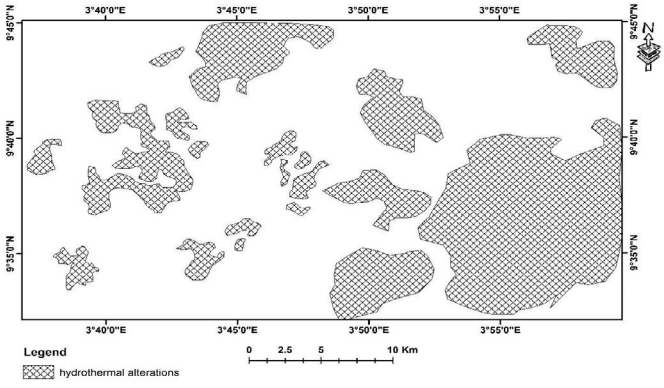

Figure 14. Delineated hydrothermal alteration zones

Lineament Interpretation

Figure 15 displays the composite shaded relief image, generated by combining azimuthal angles of 0, 45, 90, and 135 degrees. Meanwhile, Figure 16 illustrates the resultant lineament map, unveiling distinct structural orientations within the study area. These orientations are primarily oriented in the NNE-SSW, NE-SW, and NW-SE directions, as depicted in the accompanying rose diagram (Figure 17). Of notable significance is the prevalence of lineaments trending in the NE-SW direction, which emerges as the dominant structural trend. Consequently, it is inferred that these NE-SW trending lineaments play a pivotal role in controlling mineralization processes within the studied region. This orientation aligns closely with the regional structural trend previously identified in Kaiama (Ige *et al.* 2022). Kaiama is located in close proximity to a significant fault system known as the Anka Yauri Iseyin (AYI) fault, which traverses Nigeria in a dextral manner and follows a NE-SW direction (Garba, 2003). Consequently, it is highly likely that the prevailing dominant structural orientation in the study area, trending NNE-SSW, is a subsidiary feature of this major fracture system. Field investigations further corroborate that a significant portion of the NE-SW to NNE-SSW trending lineaments aligns closely with dextral strike-slip faults and shear zones within the mineralization zones. Additionally, some of these lineaments coincide with the presence of joints and fractures.

The lineament density map highlights regions characterized by high structural density. High-density zones are discernible in the northeast, central, southwest, and northwestern sectors of the study area. These particular areas are regarded as the most promising and feasible zones for mineral prospecting. Importantly, they are closely linked with lineaments exhibiting a NE-SW trending orientation. The superimposition of identified mineralization points onto the lineament density map reveals a strong correlation with areas characterized by medium to high lineament density (Figure 18). When these mineralization points are overlaid onto the geological map, it becomes evident that regions exhibiting high-density lineaments are notably associated with talc schist in the northern sector, mylonites along the southwestern boundary, as well as fine-grained granites and granite gneiss. These regions can be further studied in detail to determine the full mineralization potentials of the region.

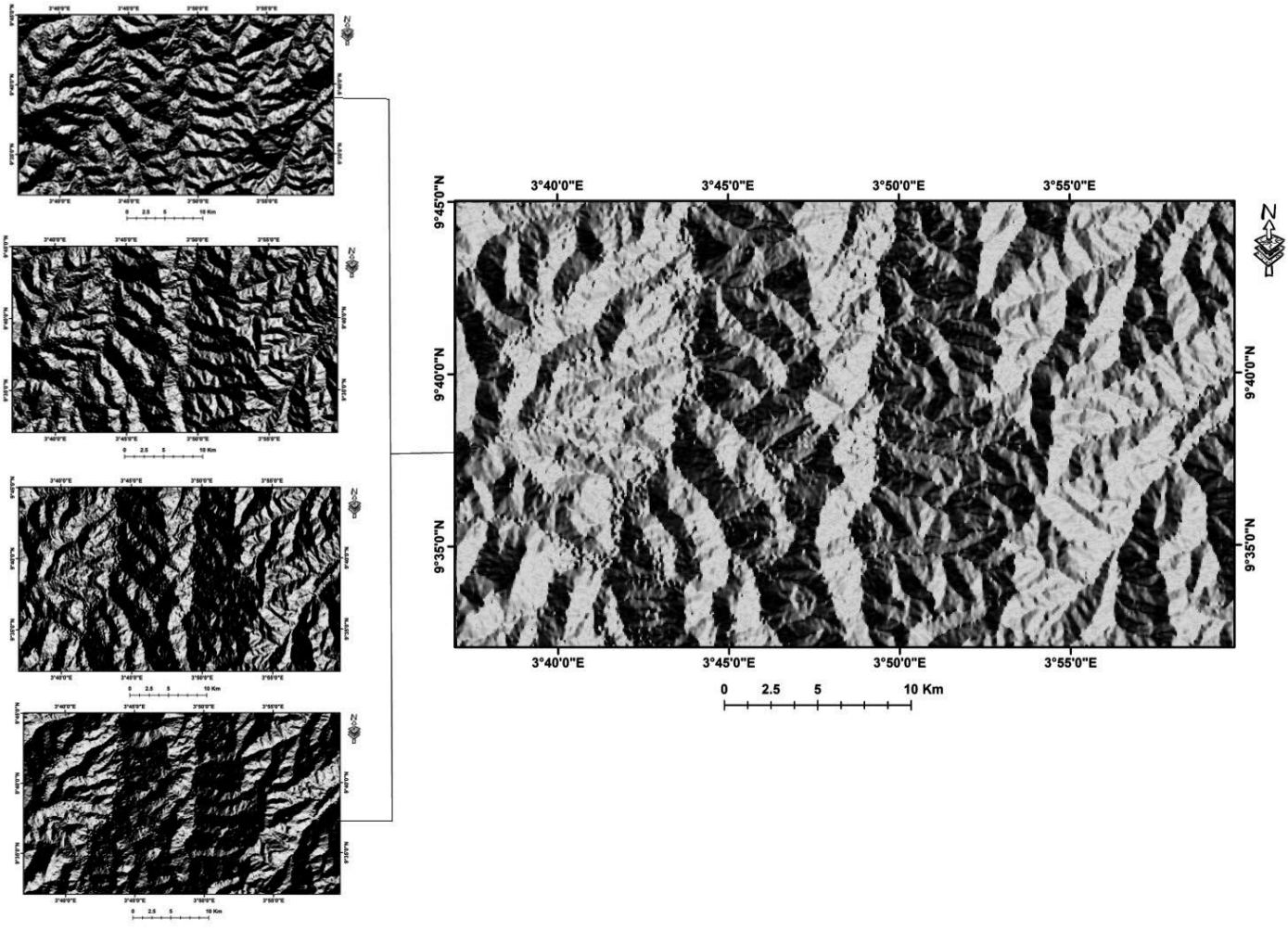

Figure 15. Combined azimuths of 0, 45, 90 and 135 degrees for lineament extraction

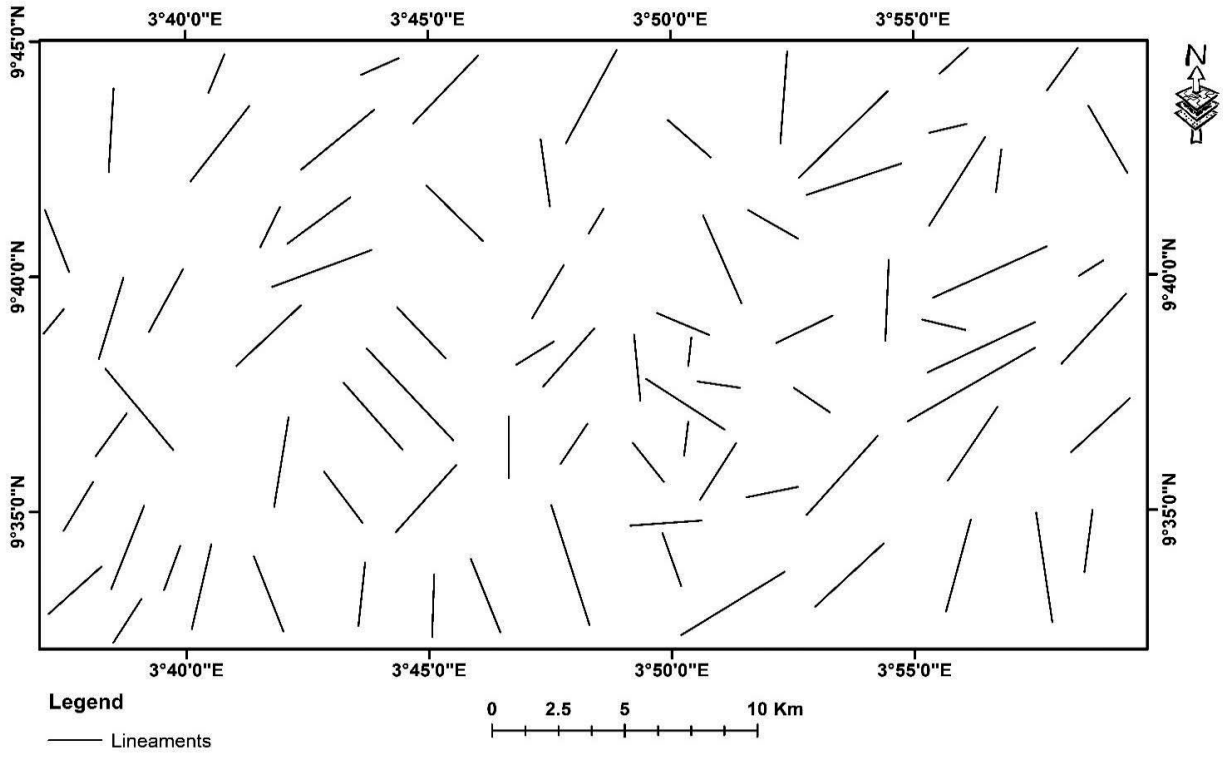

Figure 16. Extracted lineaments from combined azimuths of 0, 45, 90 and 135 degrees

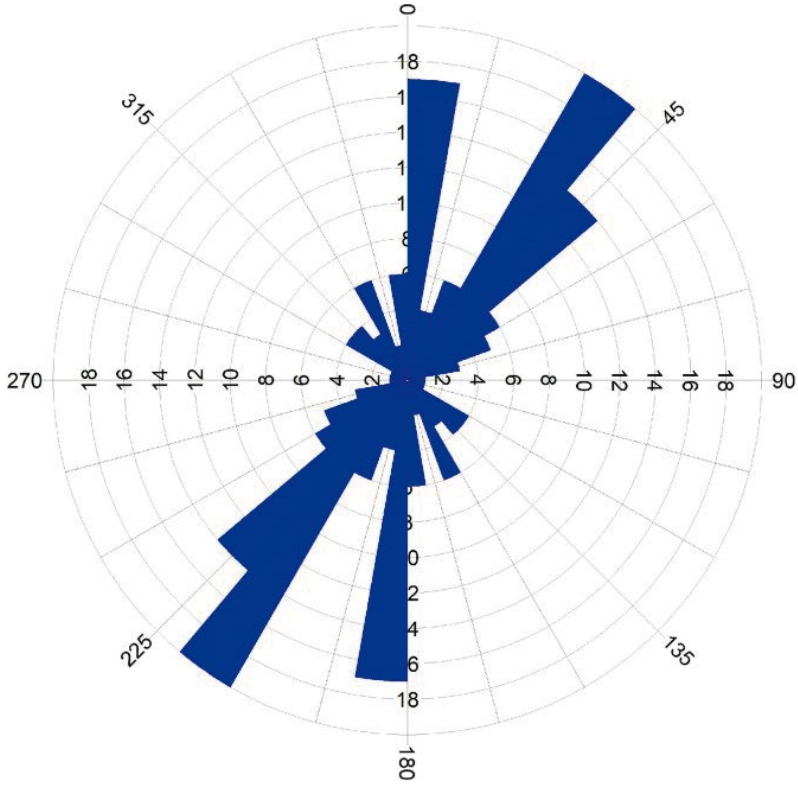

Rose Diagram

Statistical Summary

Calculation Method:	Frequency
Class Interval:	10.0 Degrees
Azimuth Filtering:	Deactivated
Data Type:	Bidirectional
Population:	104
Total Length of All Lineations:	208.0
Maximum Bin Population:	20.0
Mean Bin Population:	5.78
Standard Deviation of Bin Population:	5.49
Maximum Bin Population (%):	9.62
Mean Bin Population (%):	2.78
Standard Deviation of Bin Population (%):	2.64
Maximum Bin Length:	20.0
Mean Bin Length:	5.78
Standard Deviation of Bin Lengths:	5.49
Maximum Bin Length (%):	9.62
Mean Bin Length (%):	2.78
Standard Deviation of Bin Lengths (%):	2.64
Vector Mean:	24.0 Degrees
	203.99 Degrees
Confidence Interval:	10.5 Degrees
	(80 Percent)
R-mag:	0.46

Figure 17. Rose diagram of lineaments showing dominant orientation in NNE-SSW, NE-SW, and NW-SE

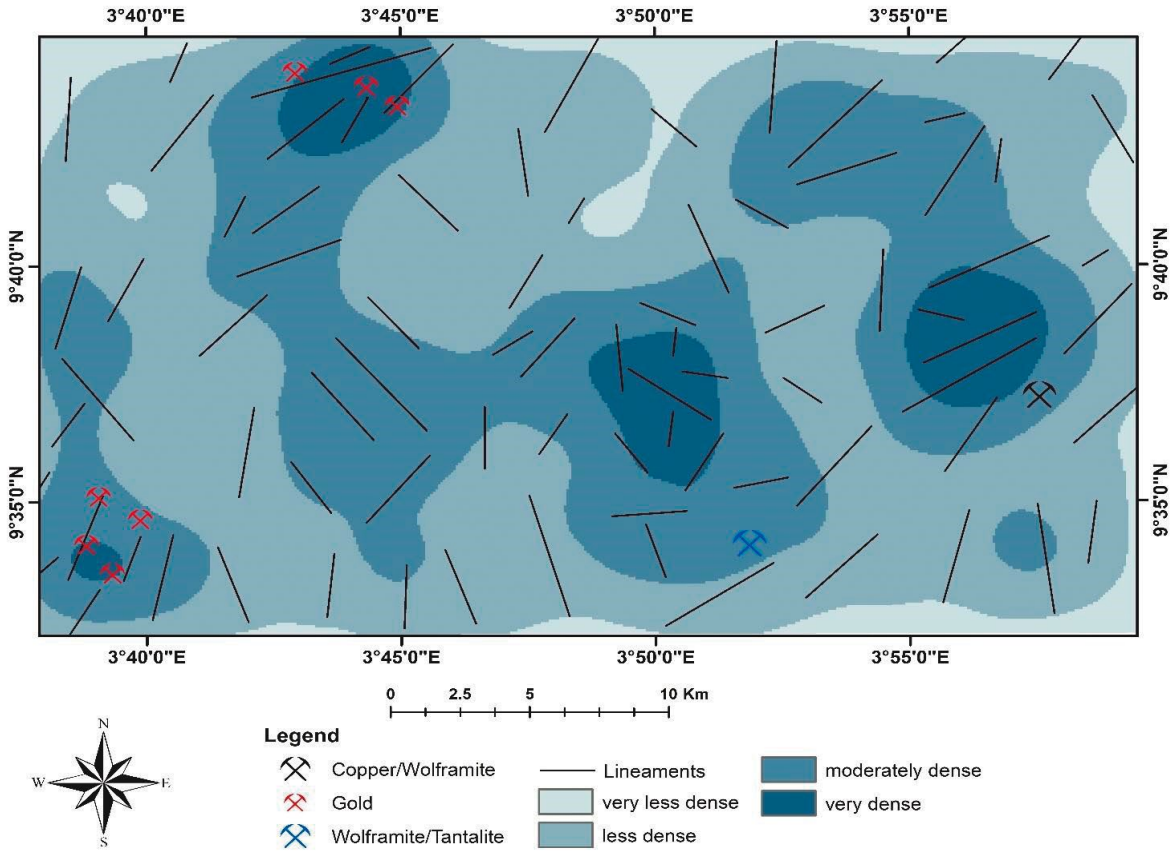

Figure 18. Lineament density map superimposed with lineaments and mineralization sites within the study area

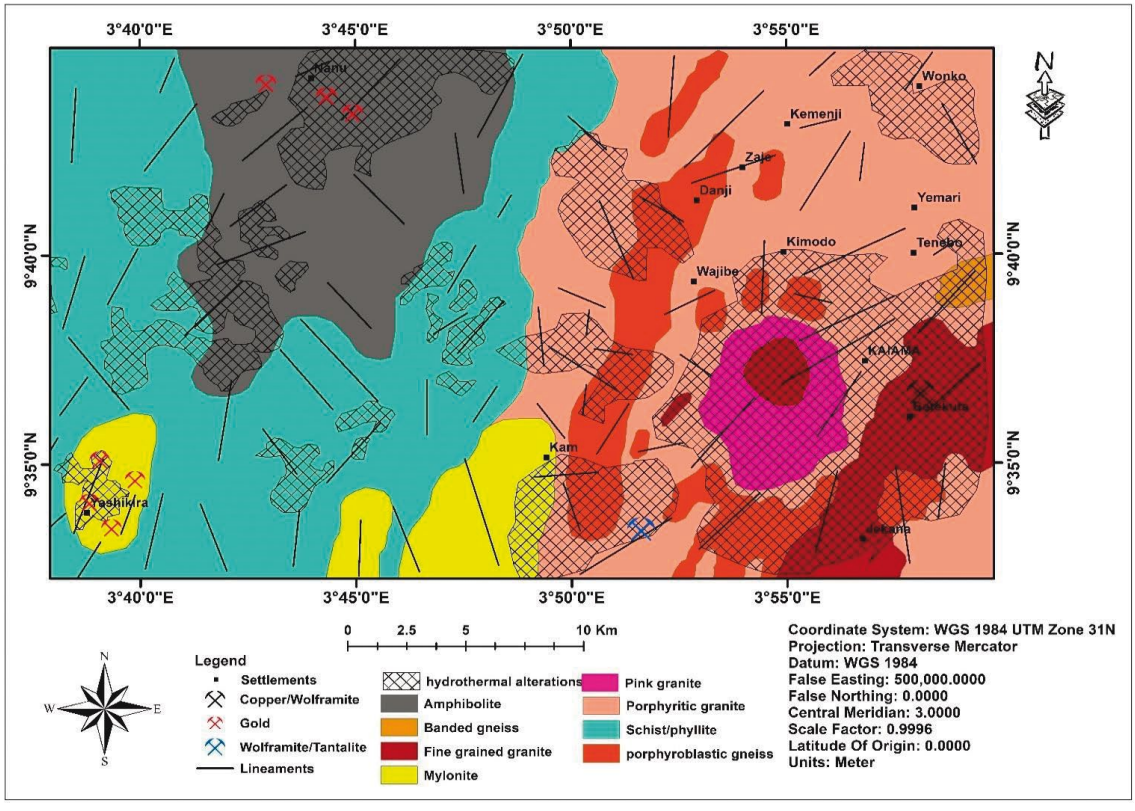

Figure 19. Integration of hydrothermal alteration zones, mining sites, extracted lineaments on the geological map of the study area.

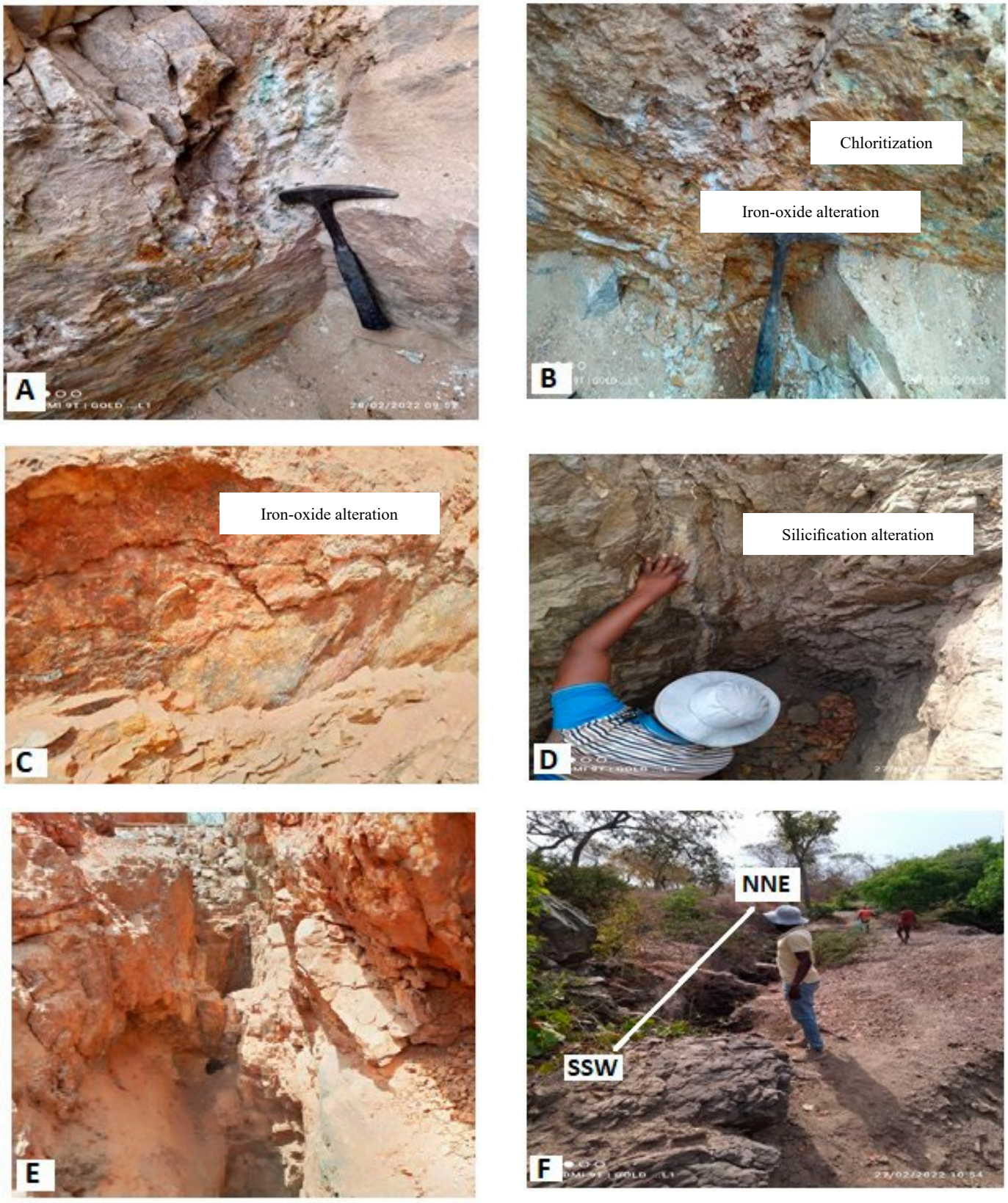

Figure 20. A. Chloritization and Silicification in Wall Rock Alteration of Porphyritic Granite at a Copper Mining Locale, B. Wall Rock Alteration in Porphyritic Granite at a Copper Mining Site with Prominent Chloritization and Silicification, C. Hematitization (Iron Oxide Alteration) in Wall Rock Alteration of Mylonite at a Gold Mining Area, D. Silicification Along the Margins of a Quartz Vein from a Gold Mining Location Hosted by Talc Schist, E. Active Gold Mining Site Displaying Evident Iron Oxide Alteration in the Wall Rocks, F. Distinct NNE-SSW Orientation Observed at a Gold Mine Site

Validation of Result

In order to validate the delineated alteration zones derived from Landsat 8 OLI satellite data, a comprehensive field investigation was undertaken. The outcomes of the fieldwork unveiled the presence of propylitic and argillic alteration assemblages, along with iron-oxide alteration domains (Figure 20). These alterations were notably correlated with linear geological features exhibiting a NE-SW orientation, encompassing fault/shear zones, joints, and fractures, which exerted control over mineralization processes. In the south-western and northern most regions of the study area, the field examination successfully identified gold mineralization within a silicic alteration zone, predominantly hosted within mylonitic rock formations. When overlaying the mineralization data onto the hydrothermal alteration map (Figure 19), a distinct alignment emerged, with mineralization points either proximate to or precisely coincident with the delineated alteration zones. Furthermore, tantalite, copper, and wolframite mining sites were discerned in the eastern and southern sectors, all of which conspicuously overlaid the identified alteration zones. It was also evident that these mineralization sites were closely associated with the northeast-southwest trending geological structures, predominantly shear zones, albeit with some contributions from joints and fractures. The findings are corroborated by Figure 20, which depicts alteration zones alongside mineralization sites, ascertained through rigorous field investigations. In summation, the field observations conducted during the verification process affirm that the various processing techniques applied to the Landsat 8 OLI imagery successfully delineated hydrothermal alteration zones, which are likely to represent prospective areas for mineralization

Table 6. Field coordinates of mining sites and minerals associated

MINERALIZATION TYPE	LATITUDE	LONGITUDE	SETTLEMENT
Gold	9^0 44' 10.88"	3^0 42' 49.75"	Nanu
Gold	9^0 43' 50.38"	3^0 44' 15.72"	Nanu
Gold	9^0 43' 32.10"	3^0 44' 52.48"	Nanu
Copper/Wolframite	9^0 36' 41.67"	3^0 58' 1.80"	Betekuta
Wolframite/Tantalite	9^0 33' 31.70"	3^0 51' 32.43"	SE of Kam
Gold	9^0 34' 58.68"	3^0 38' 59.30"	Yashikira
Gold	9^0 34' 40.20"	3^0 39' 56.50"	Yashikira
Gold	9^0 33' 59.60"	3^0 38' 34.62"	Yashikira

Conclusions

The utilization of Landsat 8 OLI data in conjunction with Digital Elevation Models has demonstrated remarkable efficacy in the delineation of hydrothermal alteration regions linked to mineralization within the investigated domain. Employing image enhancement techniques, such as color composites, band ratios, and principal component analysis, has yielded conspicuous depictions of ferrous minerals and hydroxyl-altered mineral zones. Concurrently, an analysis of linear features (lineaments) has provided valuable insights into the structural controls for mineralization, predominantly characterized by an NE-SW orientation. This study has successfully identified hydrothermal alteration zones prominently characterized by argillic and propylitic alterations within regions associated with gold, copper, tantalite, and wolframite occurrences as delineated by our spatial analysis. Consequently, there exists a compelling imperative for an extensive and comprehensive investigation encompassing geochemical, geophysical, and geological methodologies within these delineated zones to ascertain their complete mineralization potential.

Funding

The research work is part of the first authors' Doctoral thesis funded by Pan African University of Life and Earth Science Institute (Including Health and Agriculture), University of Ibadan, Nigeria.

Conflict of interest

The authors declare no potential conflicts of interest regarding the publication of this paper

References

Ajibade, A. C. (1976). Provisional Classification and Correlation of Schists Belts in Northwestern Nigeria. In: Kogbe, C. A. (Ed.). *Geology of Nigeria*. Elizabethan Pub. Co., Lagos, 88-90

Ajibade, A. C. (1980). *Geotectonic Evolution of the Zungeru Region, Nigeria.* [Unpublished Ph.D. Thesis: University of Wales, Aberystwyth]

Ali, A. S., & Pour, A. B. (2014). Lithological mapping and hydrothermal alteration using Landsat 8 data: a case study in Ariab mining district, Red Sea Hills, Sudan. *International Journal of Basic and Applied Sciences* 3(3), 199–208.

Alepa, V. C., Bale, R. B., Alimi, S. A. & Bonde, D. S. (2019). Reconnaissance geochemical exploration in Kaiama, North central, Nigeria. *Saudi Journal of Engineering and Technology*, 4(11), 457-472. DOI: 10.36348/sjeat.2019.v04i11.003

Alepa, V. C., Alimi, S. A., Babatunde, A. P., Andongma, T. W., & Bonde, D. S. (2019). Geostatistical Analysis of Mineral Deposit Associations using Soil, Stream Sediment, and Vein Geochemical Data from Kaiama, Northcentral Nigeria. *Saudi Journal of Engineering and Technology*, 4(9), 345-356. DOI:10.36348/SJET.2019.v04i09.003

Andongma, W. T., Gajere, J. N., Amuda, A. K., Digne Edmond, R. R., Faisal, M., & Yusuf, Y. D. (2021). Mapping of hydrothermal alterations related to gold mineralization within parts of the Malumfashi Schist Belt, North-Western Nigeria. *The Egyptian Journal of Remote Sensing and Space Science,* 24(3), 401-417. https://doi.org/10.1016/j.ejrs.2020.11.001

Abdulmalik, N., Garba, I., Abubakar, I. Y., Muhyideen, H., Agunleti, Y. S., Magaji, S. S., ... & Umaru, A. O. (2021). Application of landsat-8 operational land imager and shuttle radar topography mission-digital elevation model in the study of ikara and its environs, northwestern Nigeria. *FUDMA Journal of Sciences*, *5*(4), 308-325. https://doi.org/10.33003/fjs-2021-0504-835

Ahmadi, H., & Uygucgil, H. (2021). Targeting iron prospective within the Kabul Block (SE Afghanistan) via hydrothermal alteration mapping using remote sensing techniques. *Arabian Journal of Geosciences*, 14(3). https://doi.org/10.1007/s12517-020-06430-3

Aliyu, A., Adamu, L. M., Abdulmalik, N. F., Amuda, A. K., Umar, A. O., Umar, N., & Jungudo, S. M. (2021). Application of Remote Sensing in Lithological Discrimination of Precambrian Basement Rocks of Zungeru Area, Part of Sheet 163 (Zungeru Nw), North Central Nigeria. *FUDMA Journal of Sciences 5*(3), 390-398. https://doi.org/10.33003/fjs-2021-0503-729

Bannari, A., El-Battay, A., Saquaque, A., & Miri, A. (2016). PALSAR-FBS L-HH mode and Landsat-TM data fusion for geological mapping. *Advances in Remote Sensing,* 5(04), 246. DOI: 10.4236/ars.2016.54020

Crosta, A. P., & Moore, J. M. (1989). Enhancement of Landsat Thematic Mapper Imagery for Residual Soil Mapping in SW Minas Gerais State, Brazil: A Prospecting Case History in Greenstone Belt Terrain. *Proceedings of the 7th Thematic Conference on Remote Sensing for Exploration Geology*, 1173-1187

Caby, R., Sial, A. N., Arthaud, M., & Vauchez, A. (1991). Crustal Evolution and the Brasiliano Orogeny in Northeast Brazil. In: Dallmeyer, R. D., Lécorché, J. P. (eds) *The West African Orogens and Circum-Atlantic Correlatives*. IGCP-Project 233. Springer, Berlin, Heidelberg. https://doi.org/10.1007/978-3-642-84153-8_16

Dada, S. S., Tubosun, I. A., Lancelot, J. R., & Lar, A. U. (1993). Late Archaean U-Pb age for the reactivated basement of Northeastern Nigeria. *Journal of African Earth Sciences (and the Middle East),* 16(4), 405-412. https://doi.org/10.1016/0899-5362(93)90099-C

Dada, S. S. (1999). Geochemistry and petrogenesis of the reworked Archaean gneiss complex of northcentral Nigeria: major and trace element studies on Kaduna amphibolites and migmatite gneisses. *Global Journal of Pure & Applied Sciences*, 5, 535–543.

Dada, S. S. (2006). Proterozoic Evolution of Nigeria. In: Oshi, O. (Ed.). *The Basement Complex of Nigeria and Its Mineral Resources (A Tribute to Prof. M. A. O. Rahaman)*. Akin Jinad & Co., Ibadan, 29-44

Dada, S. S. (2008). *Proterozoic evolution of the Nigeria–Boborema province.* Geological Society, London, Special Publications, 294(1), 121–136. https://doi.org/10.1144/SP294

Danbatta, U. A. (2008). A review of the evolution and tectonic framework of the schist belts of Western Nigeria, West Africa. *African geosciences review,* 15(2), 145-158

Ducart, D. F., Silva, A. M., Toledo, C. L. B., & Assis, L. M. D. (2016). Mapping iron oxides with Landsat-8/OLI and EO-1/Hyperion imagery from the Serra Norte iron deposits in the Carajás Mineral Province, Brazil. *Brazilian Journal of Geology,* 46(03). https://doi.org/10.1590/2317-4889201620160023

Das, S., Pardeshi, S. D., Kulkarni, P. P. & Doke, A. (2018). Extraction of lineaments from different azimuth angles using geospatial techniques: a case study of Pravara basin, Maharashtra, India. *Arabian Journal of Geosciences,* 11, 160. https://doi.org/10.1007/s12517-018-3522-6

Dada, S. & Ajadi, J. (2018). *Exploiting Kwara state mineral resources for economic sustainability.* Kwara at 50: Achievements and Aspirations.

Farahbakhsh, E., Shirmard, H., Bahroudi, A., & Eslamkish, T. (2016). Fusing ASTER and QuickBird-2 satellite data for detailed investigation of porphyry copper deposits using PCA; case study of Naysian deposit, Iran. *Journal of Indian Society of Remote Sensing,* 44, 525–537. https://doi.org/10.1007/s12524-015-0516-7

Frutuoso, R., Lima, A., & Teodoro, A. C. (2021). Application of remote sensing data in gold exploration: targeting hydrothermal alteration using Landsat 8 imagery in northern Portugal. *Arabian Journal of Geosciences,* 14(6). https://doi.org/10.1007/s12517-021-06786-0

Garba, I. (2003). Geochemical Discrimination of Newly Discovered Rare Metal Bearing and Barren Pegmatites in the Pan-African (600 + 150 Ma) Basement of Northern Nigeria. *Applied Earth Science Transaction Institute of Mining and Mettallurgy*, 112, B287-B291. https://doi.org/10.1179/037174503225011270

Gupta, R. P. (2017). *Remote sensing geology.* Springer, second edition. https://doi.org/10.1007/978-3-662-05283-9

Guha, S., & Govil, H. (2020). Evaluation of ASTER TIR data-based lithological indices in Malanjkhand Copper Mines of Madhya Pradesh, India. *Applied Earth Science,* 129(1), 3-8. DOI: 10.1080/25726838.2019.1684018

Gaikwad, V., Singh, K., Salunke, V., & Kudnar, N. (2023). GIS-based comparative analysis of lineament extraction by using different azimuth angles: a case study of Mula river basin, Maharashtra, India. *Arabian Journal of Geosciences,* 16(9), 1–17. https://doi.org/10.1007/S12517-023-11636-2

Ige, O. O., Tende, A. W., Bale, R. B., Gajere, J. N., & Aminu, M. D. (2022). Spatial mapping of hydrothermal alterations and structural features for gold and cassiterite exploration. *Scientific African*, 17, e01307. https://doi.org/10.1016/j.sciaf.2022.e01307

Jensen, J. R. (2005). *Introductory Digital Image Processing: A Remote Sensing Perspective.* 3rd Edition, Pearson Prentice Hall, Upper Saddle River, NJ.

Koike, K., Nagano, S., & Kawaba, K. (1998). Construction and analysis of interpreted fracture planes through combination of satellite-image derived lineaments and digital elevation model data. Computers & Geosciences, 24(6), 573-583. https://doi.org/10.1016/S0098-3004(98)00021-1

Loughlin, W. P. (1991). Principal component analysis for alteration mapping. *Photogrammetry Engineering Remote Sensing,* 57, 1163–1169.

McCurry, P. (1976). The Geology of the Precambrian to Lower Paleozoic Rocks of Northern Nigeria: A Review. In: Kogbe, C. A. (Ed.). *Geology of Nigeria*, Elizabethan Publishing Company, Lagos, 15-39.

Mia, B., & Fujimitsu, Y. (2012). Mapping hydrothermal altered mineral deposits using Landsat 7 ETM+ image in and around Kuju volcano, Kyushu, Japan. *Journal of Earth System Science* 121(4), 1049–1057. https://doi.org/10.1007/s12040-012-0211-9

Masoud, A., & Koike, K. (2017). Applicability of computer-aided comprehensive tool (LINDA: LINeament Detection and Analysis) and shaded digital elevation model for characterizing and interpreting morphotectonic features from lineaments. *Computers & Geosciences,* 106, 89-100. https://doi.org/10.1016/j.cageo.2017.06.006

Meixner, J., Grimmer, J., Becker, A., Schill, E., & Kohl, T. (2018). Comparison of different digital elevation models and satellite imagery for lineament analysis: Implications for identification and spatial arrangement of fault zones in crystalline basement rocks of the southern Black Forest (Germany). *Journal of Structural Geology,* 108, 256-268. https://doi.org/10.1016/j.jsg.2017.11.006

Maleki, M., Niroomand, S., Farahbakhsh, E., Modabberi, S., & Tajeddin, H. A. (2021). Hydrothermal alteration and structural mapping of the Qolqoleh-Kasnazan shear zone in Iran using remote sensing data. *Arabian Journal of Geosciences*, *14*, 1-14. https://doi.org/10.1007/s12517-021-07920-8

Nait Amara, B., Aissa, D. E., Maouche, S., Braham, M., Machane, D., & Guessoum, N. (2019). Hydrothermal alteration mapping and structural features in the Guelma basin (Northeastern Algeria): contribution of Landsat-8 data. *Arabian Journal of Geosciences*, *12*, 1-14. https://doi.org/10.1007/s12517-019-4224-4

Oyawoye, M. O. (1972). The Basement Complex of Nigeria. In: Dessauvagie, T. F. J. and Whiteman, A. J. (Eds.). *African Geology*, University of Ibadan Press, Ibadan, 67-99.

Osinowo, O. O., Gomy, A., & Isseini, M. (2021). Mapping hydrothermal alteration mineral deposits from Landsat 8 satellite data in Pala, Mayo Kebbi Region, Southwestern Chad. *Scientific African,* 11, e00687. https://doi.org/10.1016/j.sciaf.2020.e00687

Ombiro, S. O., Olatunji, A. S., Mathu, E. M., & Ajayi, T. R. (2021). Application of remote sensing in mapping hydrothermally altered zones in a highly vegetative area–A case study of Lolgorien, Narok County, Kenya. *Indian Journal of Science and Technology*, *14*(9), 810-825. https://doi.org/10.17485/IJST/v14i9.68

Pour, A. B., & Hashim, M. (2011). Identification of hydrothermal alteration minerals for exploring of porphyry copper deposit using ASTER data, SE Iran. *Journal of Asian Earth Sciences,* 42(6), 1309-1323. https://doi.org/10.1016/j.jseaes.2011.07.017

Pour, A. B., Hashim, M., & Van Genderen, J. (2013). Detection of hydrothermal alteration zones in a tropical region using satellite remote sensing data: Bau goldfield, Sarawak, Malaysia. *Ore Geology Reviews*, 54, 181-196. https://doi.org/10.1016/j.oregeorev.2013.03.010

Pour, A. B., & Hashim, M. (2015). Hydrothermal alteration mapping from Landsat-8 data, Sar Cheshmeh copper mining district, south-eastern Islamic Republic of Iran. *Journal of Taibah University for Science*, 9(2), 155–166. https://doi.org/10.1016/j.jtusci.2014.11.008

Rahaman, M. A. (1988). Recent Advances in the Study of the Basement Complex of Nigeria. In: *Precambrian Geology of Nigeria*. Geological Survey of Nigeria Publication, 11-43.

Sabins, F. F. (1999). Remote sensing for mineral exploration. *Ore Geology Reviews* 14(3–4), 157–183. https://doi.org/10.1016/S0169-1368(99)00007-4

Sekandari, M., Masoumi, I., Beiranvand Pour, A., Muslim, A. M., Rahmani, O., Hashim, M., Zoheir, B., Pradhan, B., Misra, A., & Aminpour, S. M. (2020). Application of Landsat-8, Sentinel-2, ASTER and WorldView-3 Spectral Imagery for Exploration of Carbonate-Hosted Pb-Zn Deposits in the Central Iranian Terrane (CIT). *Remote Sensing,* 12(8), 1239. https://doi.org/10.3390/rs12081239

Takodjou Wambo, J. D., Pour, A. B., Ganno, S., Asimow, P. D., Zoheir, B., Salles, R. D. R., Nzenti, J. P., Pradhan, B., & Muslim, A. M. (2020). Identifying high potential zones of gold mineralization in a sub-tropical region using Landsat-8 and ASTER remote sensing data: A case study of the Ngoura-Colomines goldfield, eastern Cameroon. Ore Geology Reviews, 122, 103530. https://doi.org/10.1016/j.oregeorev.2020.103530

Turner, D. C. (1983). Upper Proterozoic Schist Belt in the Nigerian Sector of Pan African Province of West Africa. In: Kogbe, C.A. (Ed.). *Geology of Nigeria*, 2nd Revised Edition, Rock-view Limited, Jos, Nigeria. https://doi.org/10.1016/0301-9268

Tende, A. W., Mustapha, T., & Fru, M. I. (2022). Hybrid extraction of tectonic lineaments from digital elevation model. *Applied Geomatics* 14, 163–180. https://doi.org/10.1007/s12518-022-00422-6

Umaru, A. O., & Kankara, I. A. (2020). Utilizing Landsat-8 Sensor Operational Land Image Data for Hydrothermal Alteration Mapping Within Anka Schist Belt, Northwestern Nigeria, Researches *Reviews of the Department of Geography, Tourism and Hotel Management*, 127–149, DOI:10.5937/ZbDght2002127A

Umaru, A. O., Hamza, M., Umar, D. A., Hamman, K. I., Abdulmalik, N. F., Adamu, L., & Mbitsa, K. (2021). Mapping Tectonic Lineaments in The Pre-Cambrian Terrain of the Zuru Schist Belt, Northwestern Nigeria. *Science Forum Journal of Pure and Applied Sciences,* 21(1), 181-187. http://dx.doi.org/10.5455/sf.71057

Umaru, A. O., Okunlola, O., Danbatta, U. A., & Olisa Olusegun, G. (2022). Litho-structural and hydrothermal alteration mapping for delineation of gold potential zones within Kaiama, northwestern Nigeria, using airborne magnetic and radiometric data. *Arabian Journal of Geosciences*, *15*(24), 1771. https://doi.org/10.1007/s12517-022-11048-8

Woakes, M., Ajibade, C. A., & Rahaman, M. A. (1987). Some Metallogenetic Features of the Nigerian Basement. *Journal of African Earth Sciences*, 5, 655-664. https://doi.org/10.1016/0899-5362(87)90004-2

Wang, Z., Zhou, C., & Qin, H. (2020). Detection of hydrothermal alteration zones using ASTER data in Nimu porphyry copper deposit, south Tibet, China. *Advances in Space Research,* 65(7), 1818-1830. https://doi.org/10.1016/j.asr.2020.01.008

Yekin, E. (2003). *Alteration Mapping by Remote Sensing: Application to Hasandag-Mineraliz Volcanic Complex.* [M.Sc. Thesis, The Middle East Technical University, Turkey].